PLOS | ONE

RESEARCH ARTICLE

Investigation of Ground-Level Ozone and High-Pollution Episodes in a Megacity of Eastern China

Heng Zhao[1], Shanshan Wang[2]*, Wenxin Wang[1], Rui Liu[1], Bin Zhou[1,3]*

1 Shanghai Key Laboratory of Atmospheric Particle Pollution and Prevention (LAP[3]), Department of Environmental Science & Engineering, Fudan University, Shanghai 200433, China, **2** School of Environment and Architecture, University of Shanghai for Science and Technology, Shanghai 200093, China, **3** Fudan Tyndall Centre, Fudan University, Shanghai 200433, China

* binzhou@fudan.edu.cn (BZ); shanshan.wang@usst.edu.cn (SSW)

Citation: Zhao H, Wang S, Wang W, Liu R, Zhou B (2015) Investigation of Ground-Level Ozone and High-Pollution Episodes in a Megacity of Eastern China. PLoS ONE 10(6): e0131878. doi:10.1371/journal.pone.0131878

Editor: Aijun Ding, Nanjing University, CHINA

Received: December 30, 2014

Accepted: June 9, 2015

Published: June 29, 2015

Data Availability Statement: All relevant data are within the paper.

Funding: This work was partially supported by the National Natural Science Foundation of China under grant No. 21477021, 21277029, 40975076, 41405117, Science and Technology Commission of Shanghai Municipality (Grant: 12DJ1400102), China Meteorological Administration (Grant: GYHY201106045-8), and National Hightech R&D Program ("863" Program, No. 2006AA06Z417). The funders had no role in study design, data collection and analysis, decision to publish, or preparation of the manuscript.

Abstract

Differential Optical Absorption Spectroscopy (DOAS) was used for the long-term observation of ground-level ozone (O_3) from March 2010 to March 2013 over Shanghai, China. The 1-hour average concentration of O_3 was 27.2 ± 17.0 ppbv. O_3 level increased during spring, reached the peak in late spring and early summer, and then decreased in autumn and finally dropped to the bottom in winter. The highest monthly average O3 concentration in June (41.1 ppbv) was nearly three times as high as the lowest level recorded in December (15.2 ppbv). In terms of pollution episodes, 56 hourly samples (on 14 separate days) in 2010 exceeded the 1-hour ozone limit of 200 μg/m^3 specified by the Grade II of the Chinese Ambient Air Quality Standards (CAAQS, revised GB 3095-2012). Utilizing the Hybrid Single Particle Lagrangian Integrated Trajectory (HYSPLIT) model, the primary contribution to high ozone days (HODs) was identified as the regional transportation of volatile organic compounds (VOC) and high concentrations of O_3 from the chemical industrial zone in the Jinshan district of Shanghai. HODs showed higher concentrations of HONO and NO_2 than non-episode conditions, implying that HONO at high concentration during HODs was capable of increasing the O_3 concentration. The photolysis rate of HONO was estimated, suggesting that the larger number of OH radicals resulting from high concentrations of HONO have a considerable impact on ozone concentrations.

Introduction

Ground-level ozone (O_3) is regarded as one of the most significant atmospheric photochemical products. Due to the increasing motorized traffic, industrial and agricultural activities, tropospheric ozone concentrations increased substantially in recent decades [1, 2]. Dense ozone near ground level adversely affects human health, ecological system, and cultural heritage buildings [3–5]. Studies on ground-level ozone have contributed greatly to improving urban air quality and understanding the impact of tropospheric ozone on the environment. The

Competing Interests: The authors have declared that no competing interests exist.

factors favoring concentrations of ground-level ozone include high ambient temperature, intense photochemical reactions between NO_X and VOCs, and thin boundary layer. In addition, surface ozone concentration can be strongly affected by meteorological conditions such as solar radiance, relative humidity, and wind speed [6].

Shanghai is one of the largest megacities in eastern China, experiencing rapid urbanization and industrialization. The increases of population, industrial activity, and automobiles are conducive to significantly increased emissions of VOCs and NO_x. The atmospheric abundance of these compounds subsequently influence O_3 production. High ozone episodes and related photochemistry in Shanghai have been reported in previous papers, which were usually occurred in spring and summer. Ran [7] found that spring was the most productive season for ozone, with the highest daily maximum (128 ppbv) in May 2007 in Shanghai. High ozone periods with daily maximum ozone exceeding 102 ppbv were observed typically lasting for 3~5 days at a rural site of Shanghai in August 2010 [8]. The ozone weekly cycle that higher concentrations at weekend and lower during weekdays in Shanghai urban site is caused by different NO_2/NO ratio and the rate of ozone production is a function of atmospheric VOCs/NO_x ratio [9]. Besides, previous studies showed that the ozone formation in Shanghai was limited by the VOCs concentrations [7, 10, 11]. Moreover, the complex monsoon in Shanghai significantly affects atmospheric pollution via air mass transport. Wang [12] found that the summer monsoon introduced oceanic air with lower ozone concentration to the region, and caused lower ozone mixing ratios in summer, such that peak ozone concentrations occurred during late spring at sites in the Yangtze River Delta. Therefore, as the research hotspot in atmospheric chemistry, O_3 production and destruction in Shanghai still deserve to be better understood, which is a critical prerequisite for the development of effective O_3 control strategies.

Differential Optical Absorption Spectroscopy (DOAS) is a well-established technique and has been used to measure trace gases such as O_3, NO_2, SO_2, HONO, HCHO, aromatics and halogen oxides worldwide [13–15]. Several previous studies used DOAS to measure tropospheric air pollution [16–21]. Premuda [22] analyzed the vertical structure of O_3 and NO_2 concentrations measured by DOAS on the Castel Porziano Presidential Estate pine forest near a metropolitan area. Observation for SO_2, NO_2, and O_3 concentrations by the DOAS technique in an urban semi-industrial area of Athens, Greece, provided the evidence of higher ozone concentrations during weekends despite lower concentrations of ozone precursors [23]. In Shanghai, the active DOAS technique was applied to measure atmospheric SO_2, NO_2, O_3, HONO, HCHO and NO_3 in previous researches [24–27].

In this study, measurements of ground-level O_3 were performed by the DOAS technique from March 2010 to March 2013 in Shanghai, China. These long-term data series were used for preliminary assessment of O_3 temporal characteristics, e.g. seasonal and diurnal patterns of O_3 concentration in Shanghai. The relationships between ozone and its photochemical precursors, such as NO_2 and HONO, are discussed with regard to ozone formation mechanism. For more detailed insight into patterns of ozone pollution, HODs (high ozone days) were analyzed with HONO trend (a significant precursor of ozone) and backward trajectory. Additionally, the production of hydroxyl radicals from photolysis of HONO was estimated, and air mass back-trajectories and meteorological parameters were used to further analysis of the contributory factors to extreme O_3 concentration.

Data and Methods

Measurement site and experimental setup

The measuring principle of a DOAS system is based on the fact that all trace gases absorb electromagnetic radiation in some part of the spectrum. The result of the absorption measurement

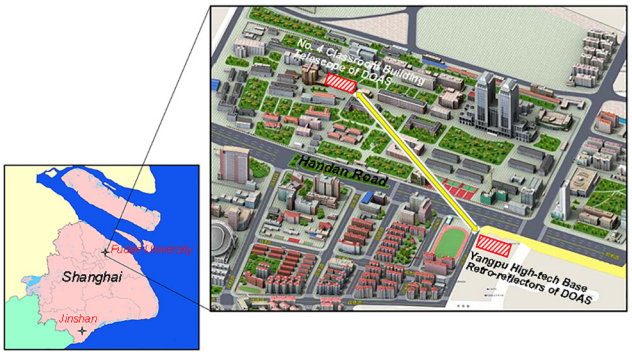

Fig 1. Overall view of the measurement site and light path of the DOAS system.

doi:10.1371/journal.pone.0131878.g001

is evaluated in terms of the correlation between the gas concentration and the amount of light absorbed, following the Lambert-Beer law:

$$I(\lambda) = \mathrm{I}_0(\lambda) \times e^{-\sigma(\lambda)cL} \quad (1)$$

Here, $\mathrm{I}_0(\lambda)$ is the reference spectrum; $\mathrm{I}(\lambda)$ is the spectrum at a distance L through the atmosphere; $\sigma(\lambda)$ is the absorption cross-section at wavelength λ; c is the concentration of gas; L is the light path length [15]. There were no specific permissions required for this experiment location, and the experiment study did not involve endangered or protected species.

The DOAS system designed and assembled by the authors consists of a telescope of diameter 210 mm as transmitter and receiver, a 150 W xenon lamp as light source, and a spectrograph (B&W TEK Inc. BRU741E-1024) with a spectral range of 200–450 nm and spectral resolution (FWHM) of 0.75nm. It was operated at the center of Fudan University (FDU: 31.3°N, 121.5°E), Shanghai, China. The transmitting/receiving telescope of the DOAS system was located on the roof of the No. 4 Classroom Building at a height of 20 m above the ground. The retro-reflectors were mounted at a height of approximately 44 m at the Yangpu High-tech Base building, which is located 0.68 km southeast of the classroom building. The measurement site and light path of the active DOAS system are shown in Fig 1. For the instrument maintenance, the surface of retro-reflectors and the window of receiver side were cleaned routinely every two weeks to scavenge the deposited dust and dirty.

The DOAS light beam travels above the campus from northwest to southeast crossing Handan Road, which is a trunk road with heavy traffic and an expressway tunnel beneath, running 300 m south of the No. 4 Classroom building. Moreover, there are several branch roads around the campus. Vehicular emissions are responsible for the major source of NO_x near the measurement site. A large petrochemical complex and fine chemistry are located in the Jinshan district, approximately 60 km southwest of the monitoring site (see Fig 1).

Data analysis

The spectra were analyzed by DOASIS software (Institute of Environmental Physics, IUP, Heidelberg University, Germany). O_3 is measured within the range 270–290 nm; NO_2 at 360–400 nm; HCHO at 313–340 nm and HONO at 340–380 nm with a 3-min temporal resolution. High-resolution absorption cross-sections of O_3 [28], NO_2 [29], HONO [30] and HCHO [31] were used in the spectra fitting (details in Table 1). Fig 2 shows the examples of DOAS fit for O_3, NO_2, HONO and HCHO. Ground-based active DOAS measurements for O_3, NO_2, HONO and HONO were conducted from March 2010 to March 2013. A total of 191 695

Table 1. Overview of DOAS analysis settings for the measured species.

Species	Cross Sections	Wavelength (nm)	Polynomial (Order)	Detection Limits[1] (ppbv)
O_3	O_3, SO_2, O_2, HCHO, CH_3CHO	270–290	3rd	3.0
NO_2	NO_2, HONO, HCHO	360–400	3rd	2.0
HONO	HONO, NO_2, HCHO, SO_2	340–380	3rd	0.2
HCHO	HCHO, SO_2, NO_2,O_3	313–340	3rd	1.0

[1] according to instruments noise in a light path of 1.36 km and 3 min integration time.

doi:10.1371/journal.pone.0131878.t001

spectra were analyzed, excluding some gaps due to maintenance of the instruments, inclement weather (e.g., fog and heavy rain), and shifts in the light path.

Meteorological data with a 5-min temporal resolution were collected at Pudong meteorological site (31.1°N, 121.5°E) in Shanghai, located approximately 10 km from the FDU site. To address the different temporal resolution between DOAS measurements and meteorological data, the meteorological data were averaged for hourly means to be discussed.

The 24-h air mass back-trajectories were calculated using the Hybrid Single Particle Lagrangian Integrated Trajectory (HYSPLIT) model (Version 4: Air Resources Laboratory,

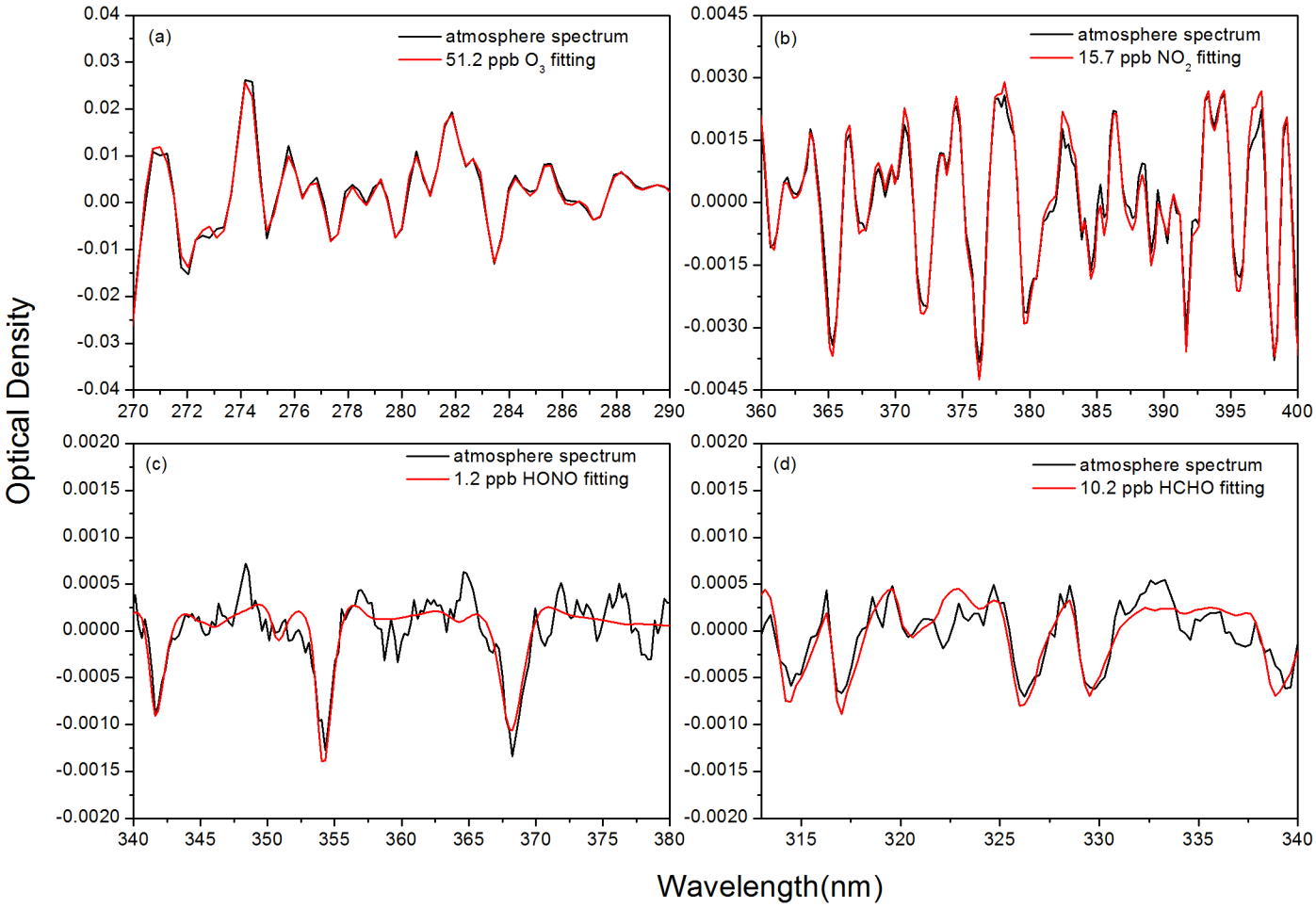

Fig 2. Examples of DOAS fitting for O_3, NO_2, HONO and HCHO.

doi:10.1371/journal.pone.0131878.g002

NOAA: National Oceanic and Atmospheric Administration, USA), which can identify the origins and transport of air masses arriving at the FDU measurement site. The meteorological data used in HYSPLIT model are the Global Data Assimilation System (GDAS) datasets with a spatial resolution of 1° × 1° and 24 vertical levels.

Results and Discussion

O_3 concentration

To demonstrate the reliability of DOAS observation, O_3 concentrations were compared with in-situ measurement by SEMC (Shanghai Environmental Monitoring Center, data from www.semc.gv.cn), located about 3 km away from FDU site, from Nov.10 to Nov.19, 2012. As shown in Fig 3 and Fig 4, the DOAS technique show a good performance in O_3 and NO_2 measurements compared to the SEMC data. The concentrations of O_3 and NO_2 measured by these two techniques generally coincided with each other, showing correlation coefficients R of 0.92 and 0.84, respectively. This reasonable difference between DOAS and in-situ measurement was probably due to the individual technique principle and distinct measurement site environment.

Time series for 8-hour and 1-hour average O_3 concentrations from March 2010 to March 2013 are displayed in Fig 5. The 8-hour moving average O_3 concentration ranged from 8.5 ppbv to 138.0 ppbv with an average of 27.2 ppbv and standard deviation of 14.8 ppbv. The maximum 8-h ozone concentration occurred from 11:00 to 19:00 on June 13, 2010, and the 8-hour moving average O_3 concentrations exceeded Grade II (160 μg/m^3, approximately 81 ppbv) of the Chinese Ambient Air Quality Standards (CAAQS, revised GB 3095–2012) among 14 days. The 1-h average O_3 concentration ranged from <1 ppbv to 167.3 ppbv with an

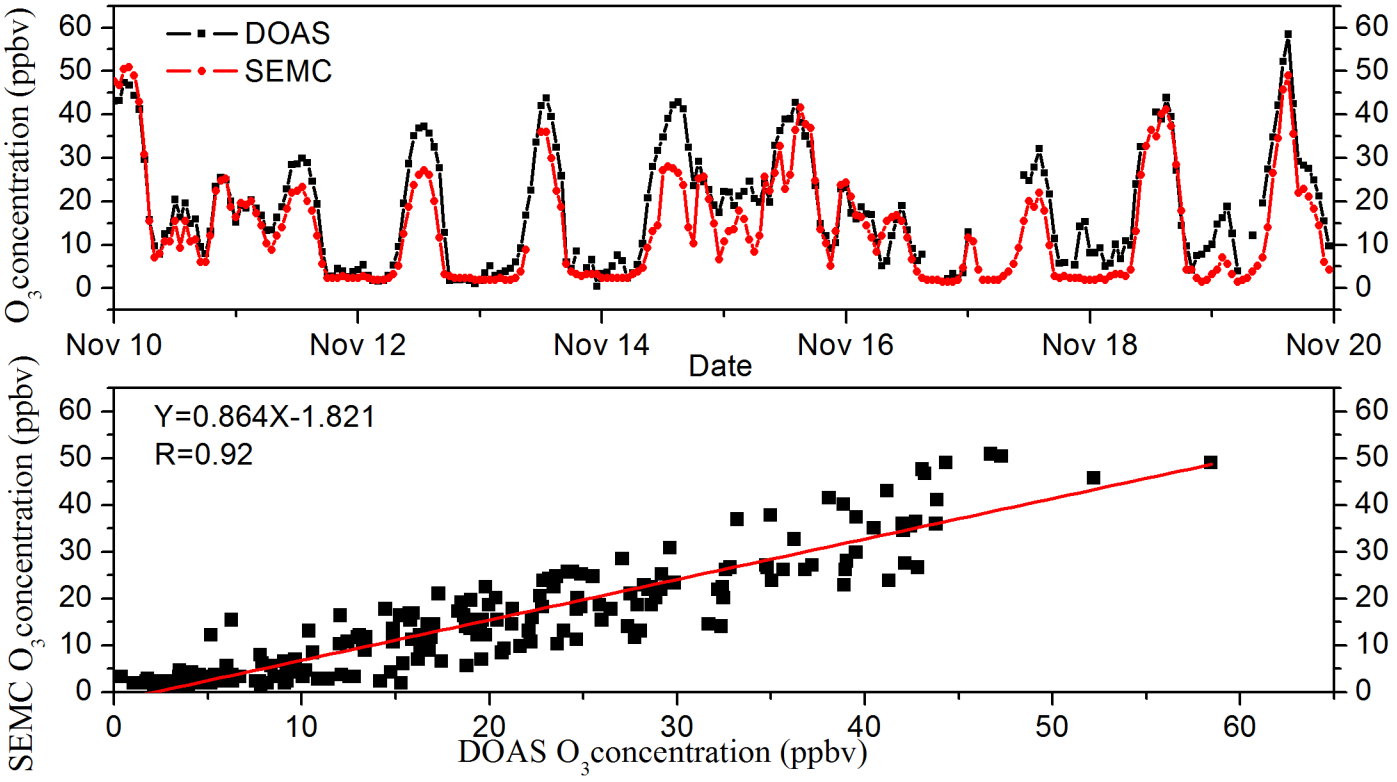

Fig 3. Comparison of O_3 data measured by DOAS and SEMC temporal variation from November 10 to 19, 2012.

doi:10.1371/journal.pone.0131878.g003

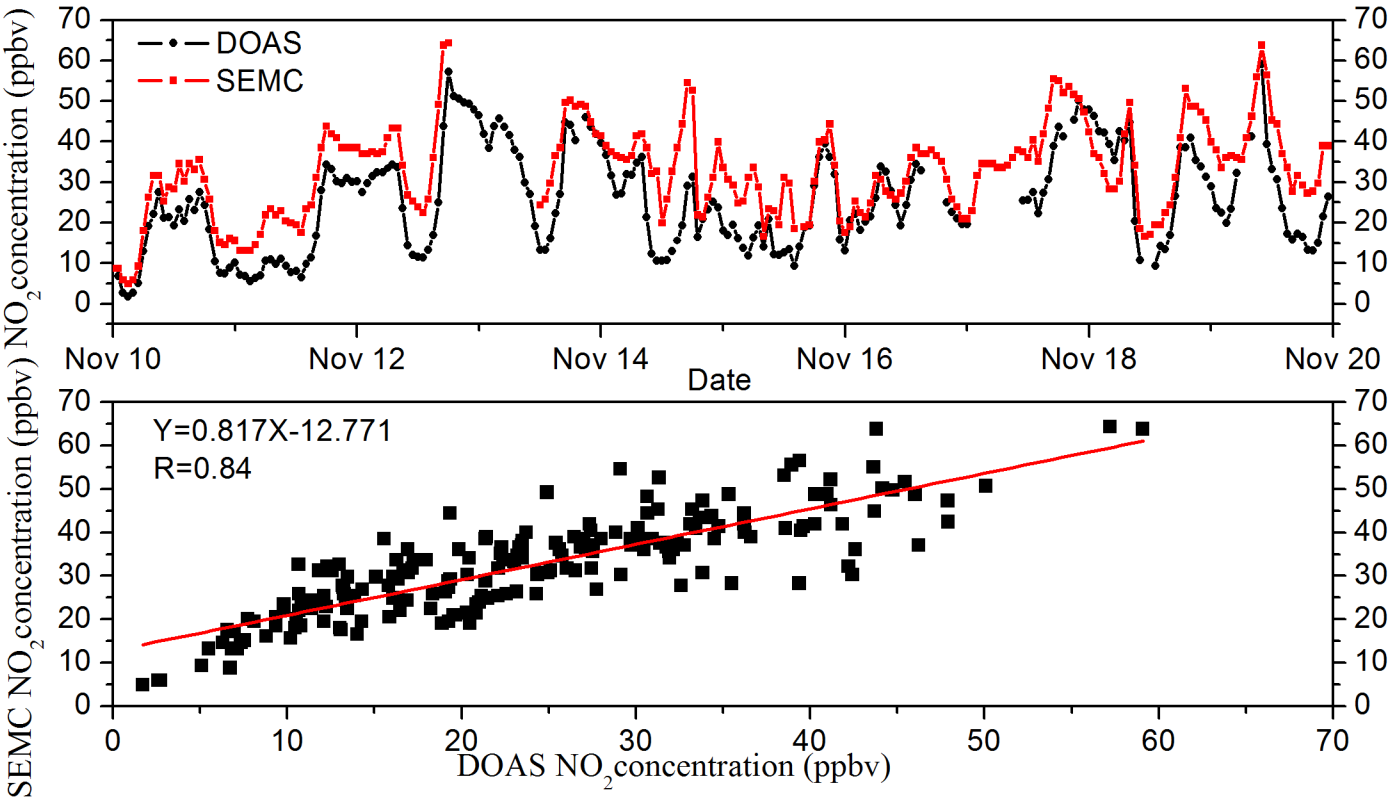

Fig 4. Relationship between concentrations measured via DOAS and SEMC.

doi:10.1371/journal.pone.0131878.g004

average of 27.2 ppbv and standard deviation of 17.0 ppbv. The highest hourly average (167.3 ppbv) occurred at 15:00 on August 13, 2010, and 56 hourly O_3 concentrations among 14 different days, shown in Fig 5(B), exceeded the Grade II threshold for hourly data (200 $\mu g/m^3$, approximately 102 ppbv). The average O_3 level in summer was significantly higher than that in winter.

In Fig 6, the counts percentages and cumulative frequency distributions of hourly average O_3 concentration in four seasons are shown. The counts of available hourly samples from spring to winter were 4080, 3074, 4881, and 4870, respectively. In the winter season, nearly 54.7% of the hourly readings were less than 20 ppbv, and only 6 hourly samples exceeded 50 ppbv (maximum 70.7 ppbv). However, during summer, only 37.7% of the hourly values were lower than 20 ppbv and the maximum concentration was extremely higher than those in other seasons. The seasonal averages in spring, summer, autumn and winter was 34.6±11.7, 31.9±17.1, 26.3±10.2 and 19.1±7.1 ppbv, respectively, which re-confirmed the fact that O_3 levels were higher in spring and summer while lower in winter at Shanghai.

Fig 7 presents the monthly variations in O_3 concentration with respect to atmospheric pressure, ambient temperature, and relative humidity. Fig 7(A) shows typical seasonal cycles, with maximum O_3 in spring and summer whereas minimum in winter. The monthly average O_3 in June (41.1 ppbv) was nearly three times as high as in December (15.2 ppbv). The average concentration gradually increased from 18.1 ppbv in January to the annual peak around 40 ppbv in May and June, and then quickly declined to around 30 ppbv in July to October, afterwards it began to decrease until December. The peaks observed in late spring and early summer have been widely reported in eastern China [7, 32, 33].

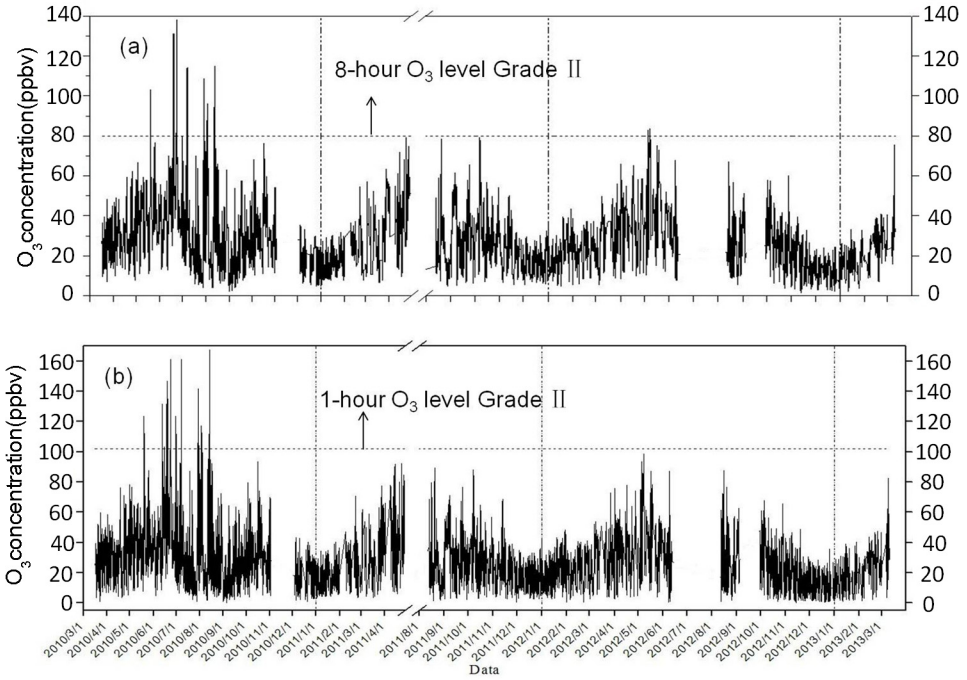

Fig 5. Time series of 8-h and 1-h average O_3 levels.

doi:10.1371/journal.pone.0131878.g005

Temperature is a critical factor in determining the rates of chemical reactions, and also is dominating to the variations of ozone concentration [34]. In our observations, O_3 concentration increased with ascending temperature until June, and then decreased with descending temperature from September to December. As expected, the atmospheric conditions in summer gradually became more favorable for photochemical formation of ozone. The positive correlation between monthly averaged temperature and ozone was found during the increase and decrease process of O_3 concentration, respectively, which agreed with the general understanding of ozone chemistry and dynamics [34, 35]. Previous studies have observed that hot and dry environment favors the production of ozone [36]. However, in the present study, the highest monthly temperature occurred in August, whereas the highest monthly O_3 concentration was in June. The decline in O_3 level from June to September might be influenced by the Asian summer monsoon, which brings oceanic air containing less ozone to the region [12, 32, 37]. Previous studies suggested that ozone concentration is negatively correlated with the relative humidity due to the reaction with water vapor, which was not found during this long term observation, as shown in Fig 7(D) [38].

Fig 8 shows the diurnal variations in hourly O_3 concentrations for different seasons between March 2010 and March 2013. Similar diurnal patterns were discovered among different seasons that higher O_3 levels appeared around 12:00~14:00, whereas lower levels occurred in the early morning from 06:00 to 08:00. O_3 concentration decreased slowly from 00:00 to 04:00 then declined significantly during early morning from 05:00 to 07:00, reaching the daily minimum. After sunrise, ozone concentration increased rapidly to its peak in the early afternoon, then decreased sharply in late afternoon. Additionally, the O_3 diurnal cycle showed much larger amplitudes in warmer seasons than during cold seasons.

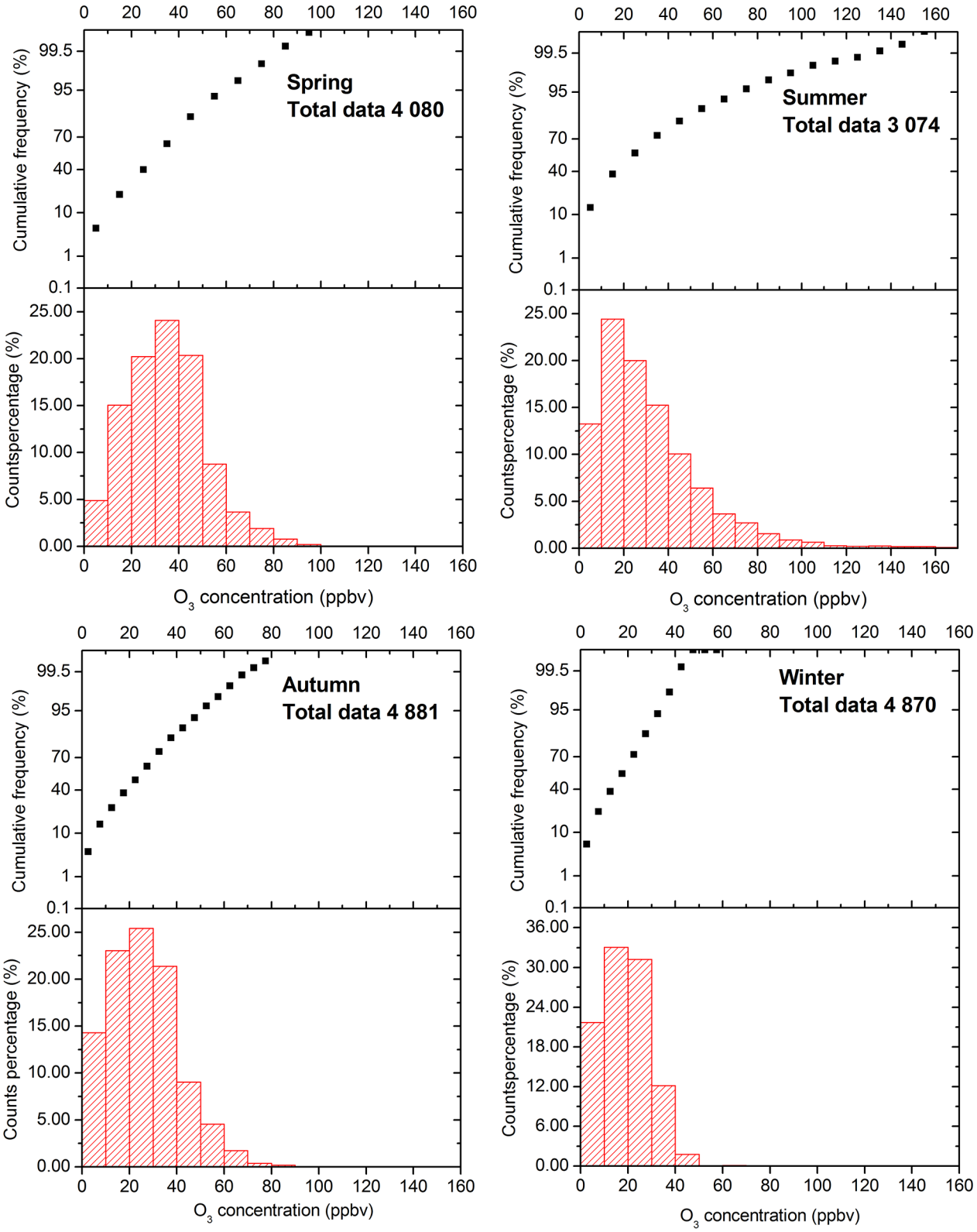

Fig 6. Frequency distribution of 1-h O_3 data for different seasons (Spring: March, April and May, Summer: June, July and August, Autumn: September, October and November, Winter: December, January and February).

doi:10.1371/journal.pone.0131878.g006

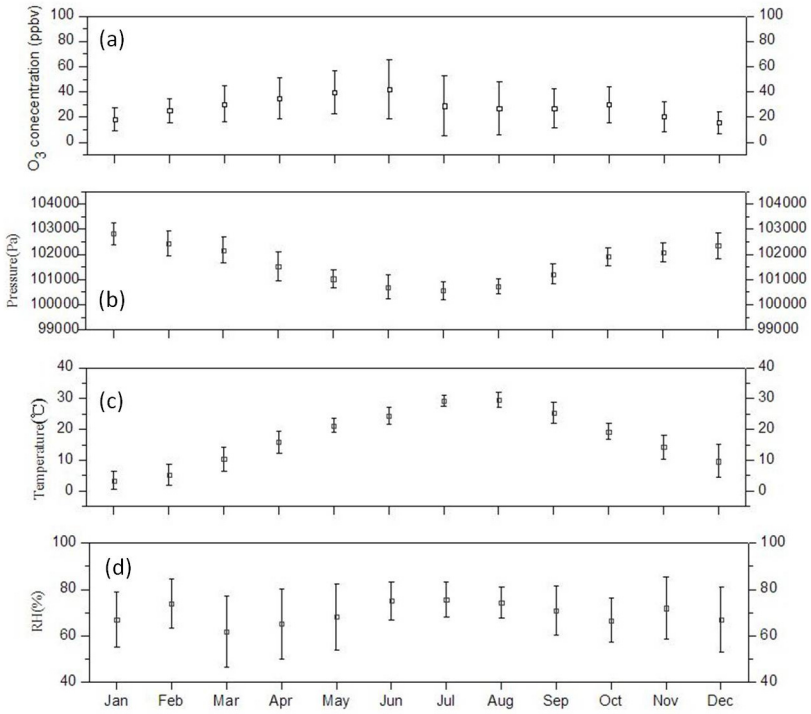

Fig 7. Monthly average of (a) O_3 concentrations, (b) pressure, (c) temperature and (d) relative humidity from March 2010 to March 2013.

doi:10.1371/journal.pone.0131878.g007

Relationships between O_3, NO_2 and HONO

O_3 is formed photochemically from the photolysis of NO_2, and O_3 reacts rapidly with NO reactions to produce NO_2. As a result, NO, NO_2, and O_3 are in photoequilibrium, with no net formation or loss of O_3. However, in the presence of VOCs, OH radicals react with VOCs to form intermediate RO_2 radicals (R3). These RO_2 radicals react with NO, which facilitate the cycling of NO to NO_2 and O_3 formation [39]. The photolysis of HONO (R2) after sunrise leads to the productive OH radicals during early morning, which may result in the net formation of O_3.

$$HONO + hv \rightarrow OH + NO\ (300nm < \lambda < 405nm) \quad (2)$$

$$OH + VOC\ (+O_2) \rightarrow RO_2 \quad (3)$$

$$RO_2 + NO \rightarrow RO + NO_2 \quad (4)$$

Fig 9 shows the diurnal cycle of NO_2, HONO, and O_3 concentrations from March 2010 to March 2013. NO_2 concentration was among the highest around 07:00 and 18:00, which can be explained by the increased vehicular emissions during the daily peak traffic periods. From 07:00 onwards, NO_2 was converted to NO and O_3 through photolysis, while NO was converted back to NO_2 reaction with O_3, which also led to O_3 consumption [40]. Unfortunately, data on NO were unavailable in this study, but it can still be speculated that NO concentration may increase with NO_2 during the early morning, owing to the increased emissions from vehicles. Thus, O_3 was mainly consumed by reaction with NO in the early morning. Additionally, weak UV intensity during the morning slowed the rate of NO_2 conversion to O_3, leading to the low concentration of O_3 observed around 06:00. The same reasons resulted in the rapid decrease of

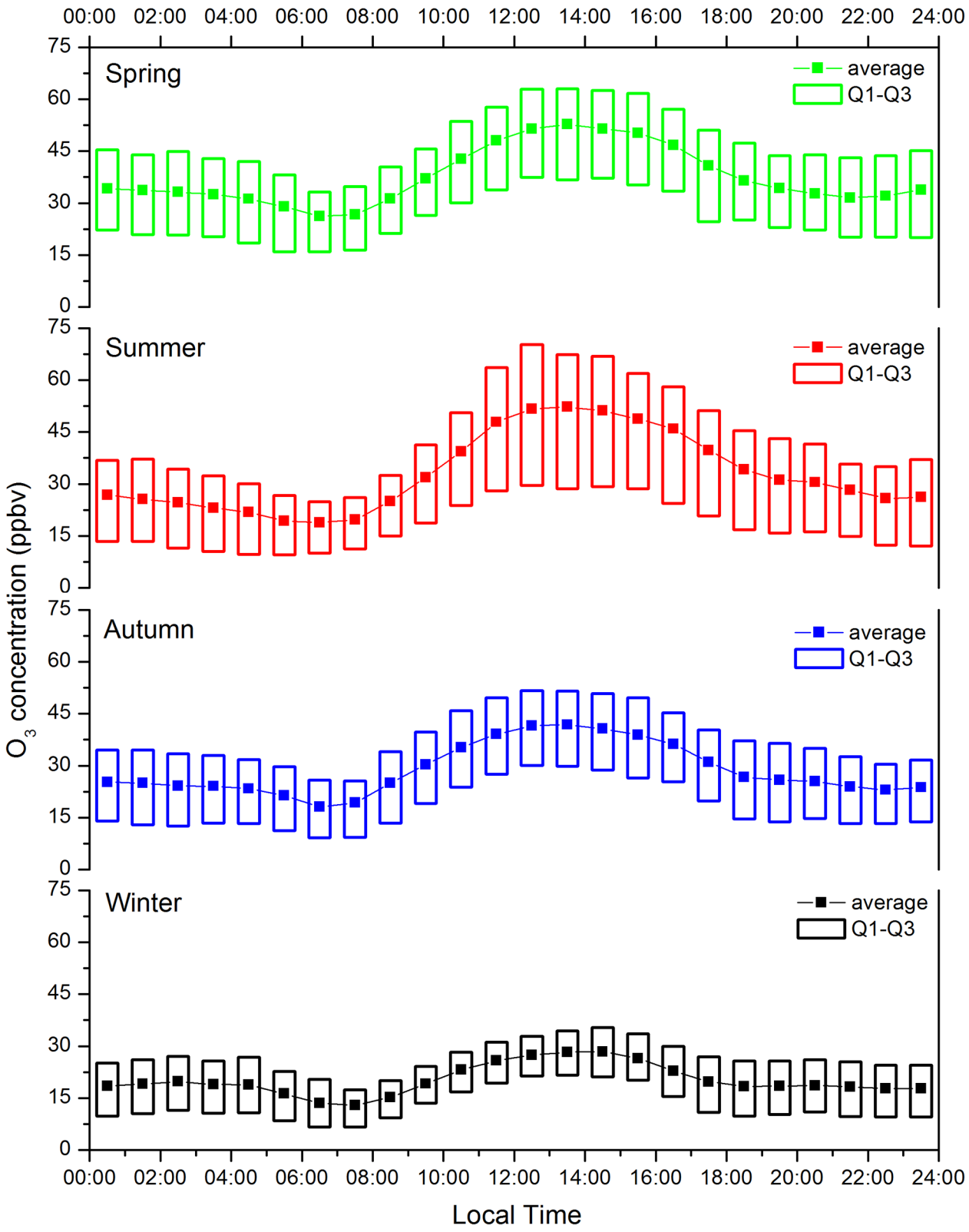

Fig 8. Diurnal cycle of averaged O_3 concentrations for different seasons.

doi:10.1371/journal.pone.0131878.g008

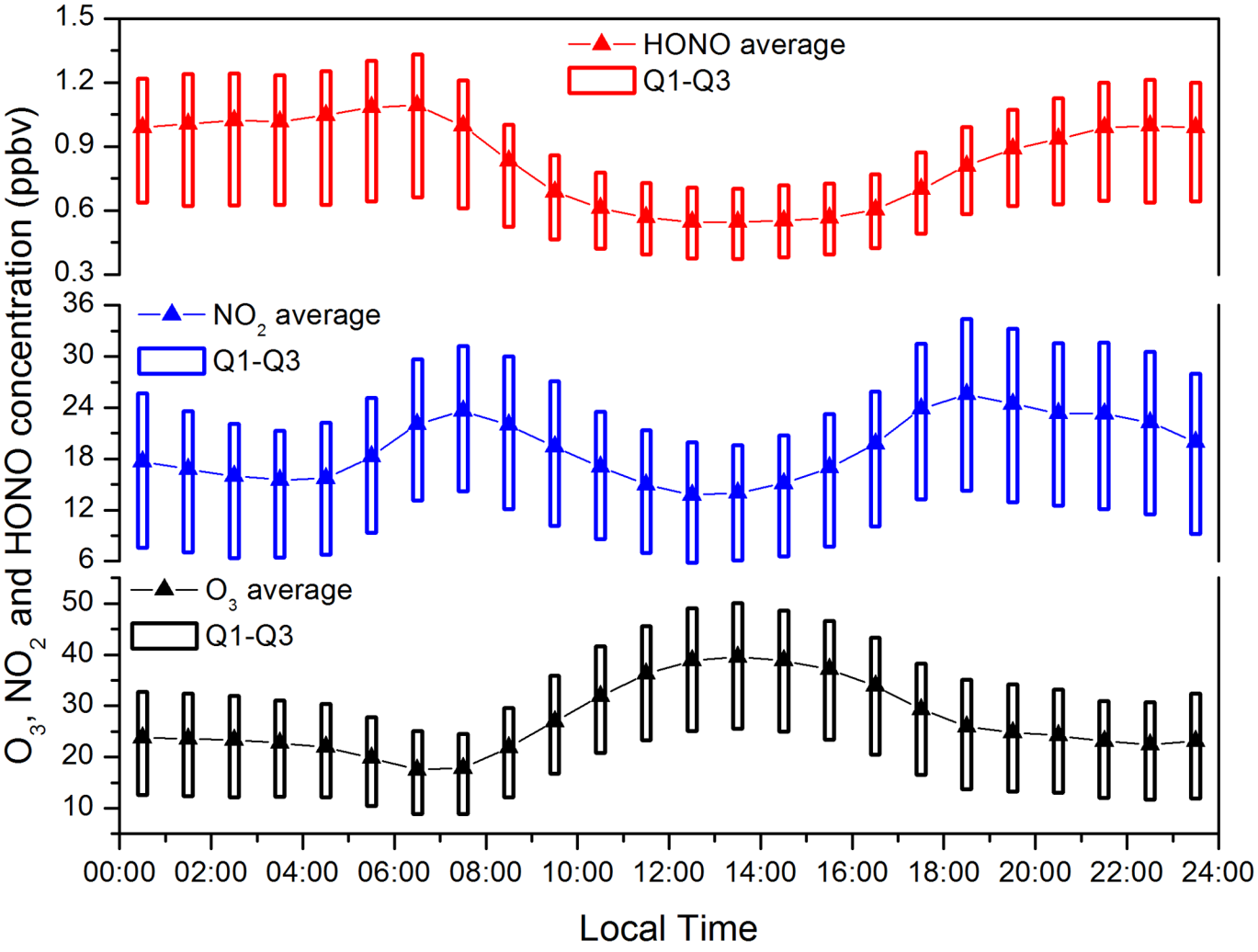

Fig 9. Diurnal cycle of averaged O_3, NO_2, and HONO concentrations during March 2010 to March 2013.

doi:10.1371/journal.pone.0131878.g009

O_3 in late afternoon. Induced by solar radiation, O_3 concentration began to increase gradually after sunrise, while NO_2 concentration continued decreasing until reaching its lowest level around 12:00. HONO concentrations dropped sharply from 6:00 to 11:00, remained low until 15:00 and then increased rapidly and remained high at night. The comparable concentration and similar diurnal pattern of HONO were also exhibited in another eastern Chinese urban site [41]. OH radicals produced by HONO photolysis could yield RO_2 radicals via the reactions with VOCs. When RO_2 radicals continuously converted NO to NO_2, O_3 reached the highest concentration in the daytime.

High ozone days

As the DOAS system failed to work in May, June, July, and August 2011, and in June, and July 2012, the present section focuses on analyzing the data in 2010. High ozone days (HODs) were defined as days during which hourly average concentration exceeding Grade II of CAAQS of O_3 (102 ppbv) appeared. Table 2 summarizes the basic condition of HODs, comprising 56 hourly O_3 concentrations exceeding the threshold on 14 different days.

Table 2. Summary of high ozone days in 2010.

Year	2010			
Month	May	June	July	August
The number of HODs	1	6	3	4
The number of exceeding hours	5	26	10	15
Max. ozone (ppbv)	123.7	161.3	161.3	167.3

doi:10.1371/journal.pone.0131878.t002

To determine the causes of high O_3 episodes, we depicted the diurnal concentrations of O_3, HONO, NO_2 and HCHO on the 14 selected HODs, together with the preceding and succeeding days for each, as well as the annual means (see Fig 10). Fig 10(A) shows a typical O_3 diurnal cycle, with daily minimum in the early morning and maximum in the early afternoon. During the episode days, ozone concentration reached 120.1 ppbv at 14:00 (about 60 and 80 ppbv higher than those during pre-/post-episode and annual mean), suggesting the occurrence of intensive photochemical reactions. HONO concentrations between 22:00 and next 06:00 during O_3 episodes were significantly higher than those during non-episode days, whereas the concentrations at noon were lower, which implies that more HONO was decomposed in daytime during O_3 episodes (Fig 10(B)). Li [42] concluded that the addition of HONO sources significantly affects HOx (HOx = OH + HO_2) in Mexico City, leading to a midday average increase in O_3 of about 6 ppb. Czader [43] found that because HONO immediately photo-dissociates during daytime, its ambient mixing ratios were only marginally altered (up to 0.5 ppbv), but increases in hydroxyl radical (OH) and ozone concentration were obtained. In Shanghai, heterogeneous reactions has been considered to be the significant contributor to HONO formation [11, 25, 44], which may further impact the ozone formation. The sensitivity simulation without heterogeneous HONO sources indicated that the heterogeneous HONO formation would enhance daytime average O_3 production by rate by ~6.8 pph h^{-1} on average in Shanghai due to the released OH via HONO photolysis [45]. Therefore, it can be inferred that HONO at high concentration during episode days was capable of increasing the O_3 concentration. For NO_2, the diurnal cycles show a morning/evening peak on episode and non-episode days alike (Fig 10(C)). The photolysis of NO_2 from the morning peak resulted in O_3 increase in daytime.

Comparison of the diurnal patterns for episode and non-episode days showed that levels of O_3, HONO, and NO_2 were higher during episodes. During the morning of HODs, increased solar radiation accelerated the rates of photolysis of NO_2 and produced more O_3, and HONO at high concentration was capable of producing abundant OH radicals via photolysis (R2). Then, OH radicals reacted with VOC to form RO_2 radicals (R3), which subsequently reacted with NO to produce NO_2 (R4). Increasing NO_2 would prohibit the reaction of NO with O_3 and reduce the consumption of O_3. Furthermore, the photolysis of NO_2 could enhance the increase of O_3. As a result of the above steps, O_3 was formed continuously and maintained high concentration.

HYSPLIT back-trajectories for high ozone days

To assess the types of air mass transport processes during these HODs, 24-h backward trajectories were analyzed via running the HYSPLIT model for HODs once a day at 12:00 Chinese Standard Time (CST) at an altitude of 500 m above ground level, presented in Fig 11.

Table 3 shows the province and direction, from which the air masses originated, along with the transport distance. On 9 of the 14 HODs, air masses originated from the southwest inland, at distances ranging from 195 km (from Jiangsu Province on June 23) to 646 km (from Jiangxi

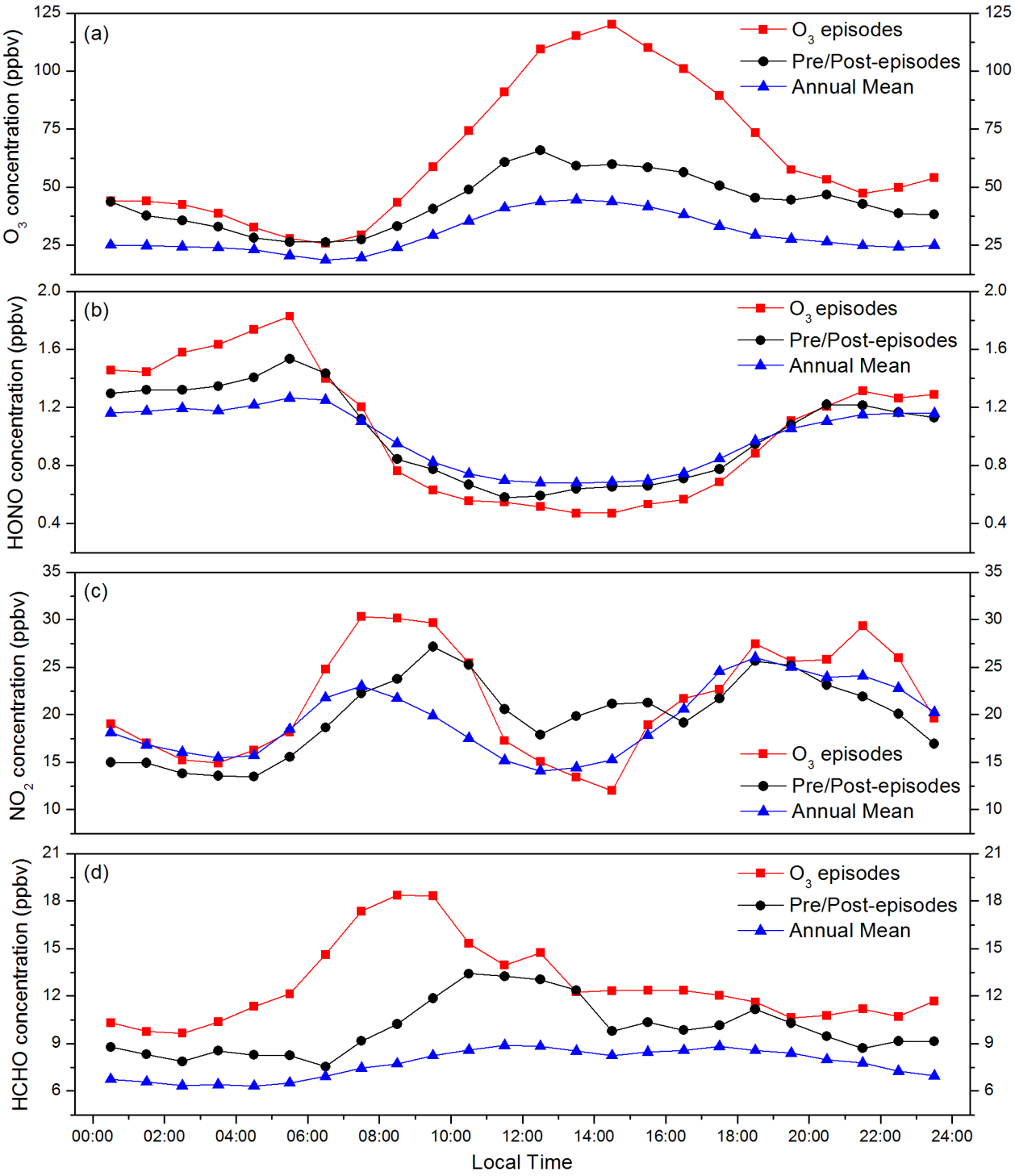

Fig 10. Diurnal variations of (a) O_3, (b) HONO, and (c) NO_2 averaged for HODs, pre-/post-episodes and annual mean in 2010.

doi:10.1371/journal.pone.0131878.g010

Province on June 30). Two air masses coming from the northwest of Shanghai originated in Anhui and Jiangsu. Only one air mass originated over the sea, beginning 145 km away and arriving in Shanghai on June 15. Southwest of the FDU campus is the Jinshan chemical industrial zone, from where numerous chemical facilities emit considerable quantities of VOCs.

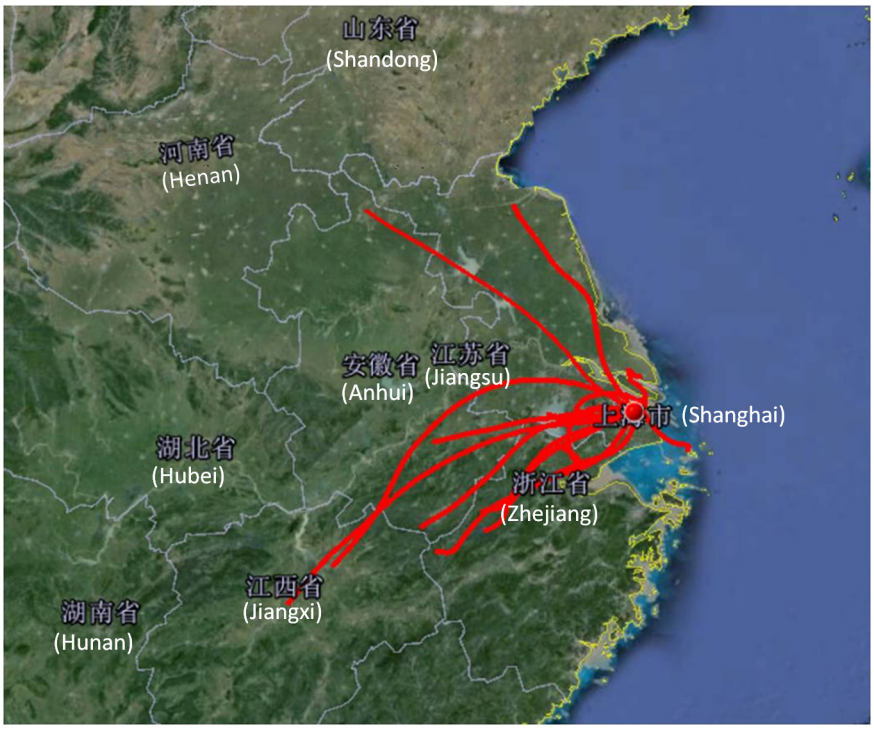

Fig 11. 24-h air mass back-trajectory during HODs.

doi:10.1371/journal.pone.0131878.g011

Based on the discussion about backward trajectories for the O_3 periods, it is very likely that pollutants such as non-methane organic compounds (NMOC) were transported from petro-chemical facilities located in Jinshan industrial zone. High concentrations of VOCs and ozone in transported air masses may be the cause of O_3 increase during high ozone episodes. Since HCHO was regarded as an important indicator of NMOC emissions, it can be inferred from Fig 10(D) that air mass originated from Jinshan area may contain more VOCs and facilitate

Table 3. Location, direction and distance of air masses trajectories in HODs.

Date	Location	Direction	Distance (km)
5.19	Anhui	Northwest	573
6.12	Jiangsu	Northwest	363
6.15	sea	Southeast	145
6.18	Zhejiang	Southwest	315
6.19	Zhejiang	Southwest	382
6.23	Jiangsu	Southwest	194
6.30	Jiangxi	Southwest	646
7.7	Jiangsu	North	112
7.29	Anhui	West	317
7.30	Jiangxi	Southwest	308
8.2	Jiangxi	Southwest	607
8.3	Zhejiang	Southwest	218
8.12	Zhejiang	Southwest	195
8.13	Anhui	Southwest	395

doi:10.1371/journal.pone.0131878.t003

the O_3 formation at downwind urban area during the O_3 episodes. Moreover, the oxygenated VOCs play important roles in O_3 formation were also demonstrated by some previous modeling and measurement studies in Shanghai [46].

Case study for high ozone days

To further understand the factors leading to extremely high ozone levels, one episode was chosen for an in-depth analysis.

Fig 12(D) presents a high ozone episode on 19 June, 2010 that lasted for 9 h, from 10:00 to 20:00. HONO and NO_2 also reached high levels on 19 June. HONO concentration peaked at 2.2 ppbv at midnight and remained approximately above 1.8 ppbv from 04:00 to 07:00 (Fig 12(C)) before high O_3 occurred. When O_3 concentration began to increase, that of NO_2 and HONO began to decrease and then remained at low concentrations. Fig 12(B) shows diurnal temperature and wind speed. The highest temperature in this case was up to 36°C. The photolysis rates of NO_2 were rapidly enhanced under strong solar radiation. NO_2 level remained relatively low at noon and produced more O_3 during this cloudless day. Additionally, the wind speed was less than 2.5 m/s, which inhibited the diffusion of O_3. HYSPLIT 24-h backward

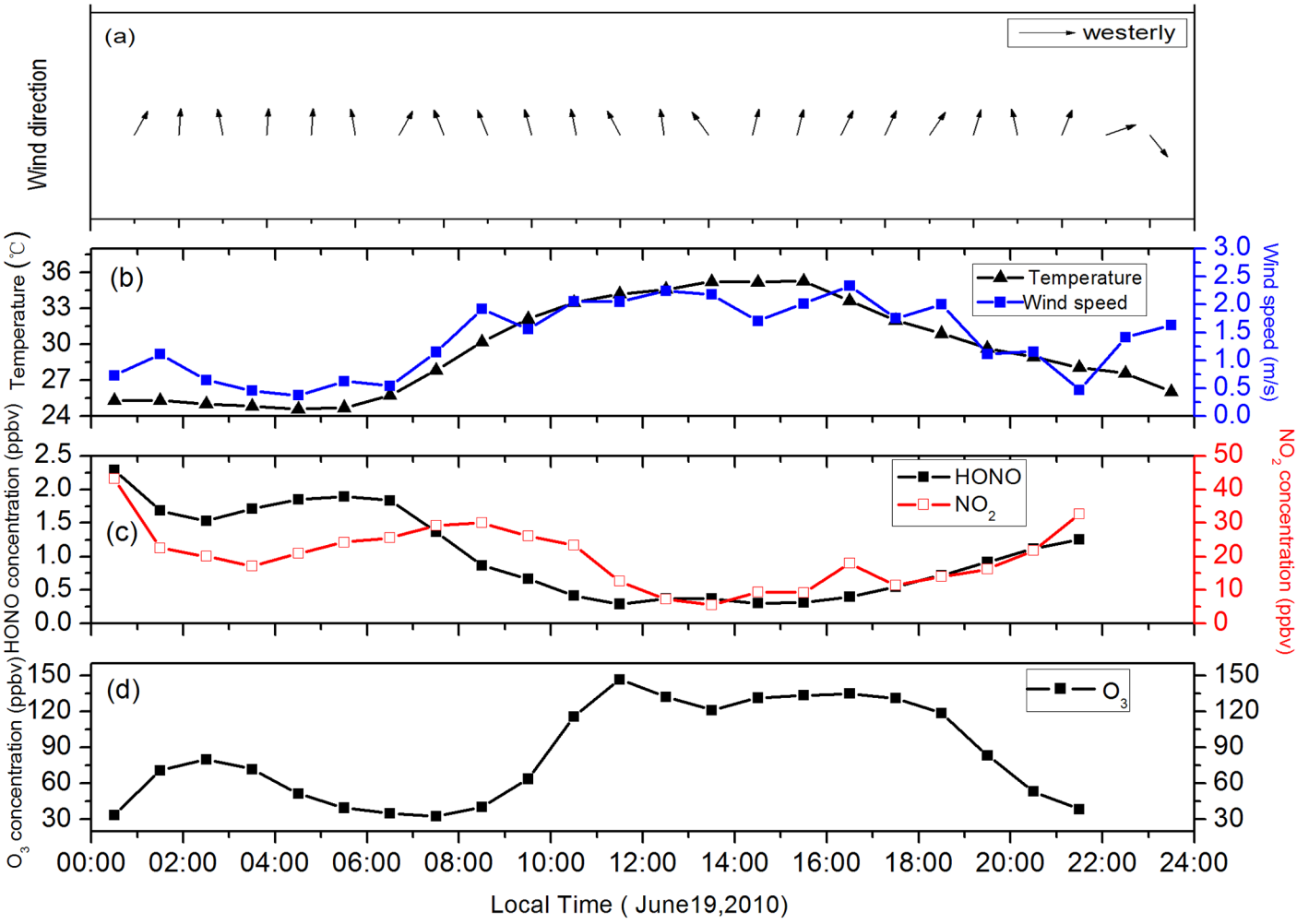

Fig 12. Wind direction (a), diurnal variations of (b) temperature and wind speed, (c) HONO and NO_2, (d) O_3 for case study.

doi:10.1371/journal.pone.0131878.g012

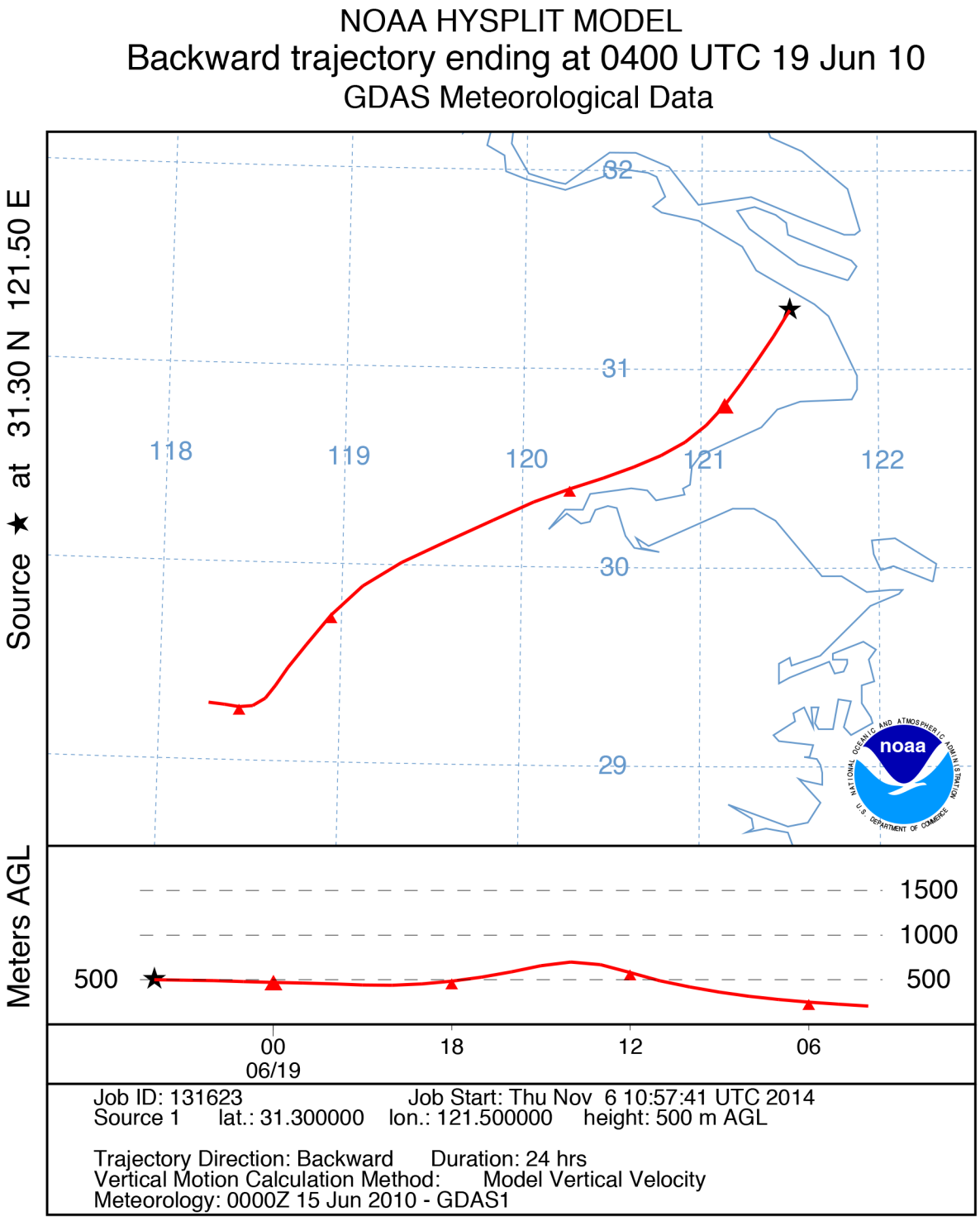

Fig 13. The 24-h air mass back-trajectory of ozone episode at 12:00 (CST) on June 19, 2010.

doi:10.1371/journal.pone.0131878.g013

trajectory analysis is presented in Fig 13. There is an obvious transport of air mass from Zhejiang at a height of 500 m. The air mass passed through Jinshan area before arriving the measurement site. As shown in Fig 12(A), the main wind direction was southwest, which are

consistent with the result of backward trajectory and further suggests that air mass from the Jinshan chemical region influenced urban O_3 concentration. The trajectory remained in the lower atmosphere until arriving at Shanghai, indicating an extensive region of stable meteorological conditions.

The photolysis of HONO was estimated from June 19 to 21, 2010 by the Tropospheric Ultraviolet and Visible (TUV) Radiation Model (http://cprm.acd.ucar.edu/Models/TUV/). The production of OH radical from HONO photolysis was obtained from the modeled photolysis frequencies, J(HONO), and the mixing ratios of HONO by R5 [47].

$$P_{OH} = J(HONO) \times [HONO] \quad (5)$$

Fig 14 shows the rates of HONO photolysis and OH radical production, as well as concentrations of O_3 and HONO for June 19–21, 2010. The concentrations of O_3 and HONO on June 19 were much higher than on June 20 and 21. The production of OH radicals on June 19 (the maximum 3.8×10^8 molec cm^{-3} s^{-1}) was significantly greater than June 20 (the maximum 2.8×10^8 molec cm^{-3} s^{-1}) and June 21 (the maximum 2.7×10^8 molec cm^{-3} s^{-1}). High concentrations of HONO produced more OH radicals, which have a greater impact on ozone concentrations.

In this case, the sunny and hot conditions facilitated NO_2 photolysis to form O_3; the low wind speed inhibited the diffusion of O_3; the transfer of air mass through the Jinshan chemical industrial zone influenced urban O_3 concentration; the additional OH radicals resulting from high concentration of HONO were capable of increasing the O_3 concentration.

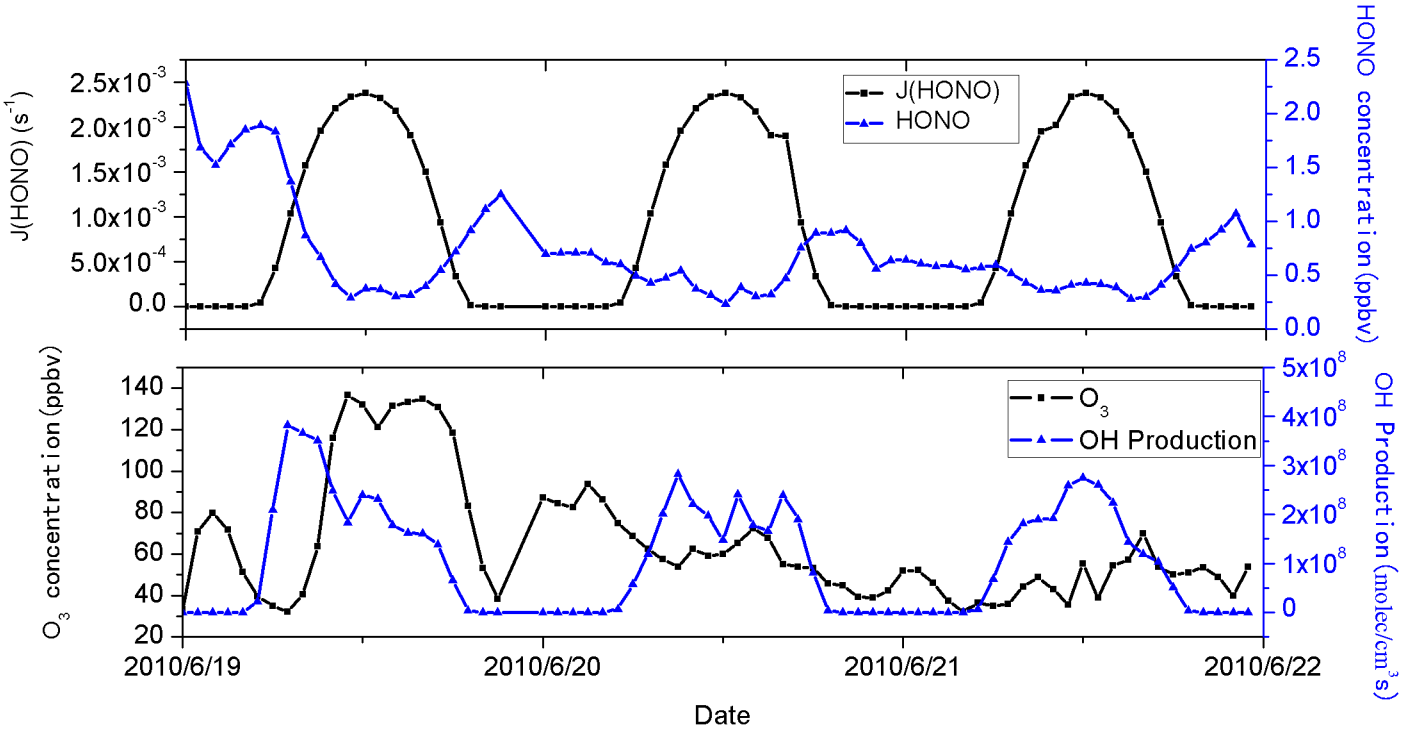

Fig 14. Rate of HONO photolysis and OH radical production, and concentrations of O_3 and HONO from June 19 to June 21, 2010.

doi:10.1371/journal.pone.0131878.g014

Conclusions

Utilizing the DOAS technique, a long-term measurement of ground-level ozone was originally performed from 2010 to 2013 over Shanghai, China. Good correlation with SEMC data suggests that the results measured by DOAS method are reliable (R = 0.92 for O_3 and R = 0.84 for NO_2). In our study, 56 hourly concentrations (on 14 separate days) in 2010 were found to exceed the Grade II limit of 200 $\mu g/m^3$ specified for 1-hour ozone concentration. Generally, the 1-hour average concentrations of O_3 were 27.2 ± 17.0 ppbv. Considering seasonal variability, O_3 levels in late spring and early summer were the highest, and the lowest in winter. The highest monthly average O_3 concentration in June (41.1 ppbv) was nearly three times as high as the lowest level recorded in December (15.2 ppbv). Seasonal and diurnal patterns of surface ozone were consistent with previous studies and were intimately associated with meteorological factors.

HODs were analyzed to establish the formation mechanism of high-ozone episodes, revealing higher levels of precursory species for O_3, including HONO and NO_2, on ozone-polluted days than on non-episode days. Photolysis of HONO can generate OH radicals, which further react with VOCs to produce RO_2 radical. New formation of radicals consumed NO and produced NO_2, resulting in further generation of ozone. Twenty-four-hour back-trajectory analysis showed that most of the air masses during HODs passed through the area occupied by the Jinshan chemical industry, which is a source of considerable VOC emissions. The provision of volatile organic compounds in Jinshan facilitates reaction with OH radicals, converting NO to NO_2, resulting in increased ozone concentration.

The case study also illustrated the obvious influence of meteorological factors on ozone concentration. The occurrence of high O_3 concentrations during daytime was attributed to the relatively high temperature, which favor the photochemical reactions to produce O_3. Furthermore, the stable meteorological conditions, characterized by low wind-speed and compressed boundary layer, inhibited ozone dispersion. Air masses during high O_3 episodes were transported through the chemical industrial region of Jinshan to the measurement site. The TUV Radiation Model suggests that high concentrations of HONO produced more OH radicals, which greatly increase ozone concentrations, in estimation of the photolysis rate of HONO.

Author Contributions

Conceived and designed the experiments: HZ SSW BZ. Performed the experiments: HZ SSW WXW RL. Analyzed the data: HZ. Contributed reagents/materials/analysis tools: HZ SSW BZ. Wrote the paper: HZ SSW.

References

1. Sicard P, Coddeville P, Galloo JC (2009) Near-surface ozone and trends at rural stations in France over the 1995–2003 period. Environ Monit Assess 156, 141–157. doi: 10.1007/s10661-008-0470-8 PMID: 18665450
2. Sicard P, De Marco A, Troussier F, Renou C, Vas N, Paoletti E, et al. (2013) Decrease in ozone mean concentrations at Mediterranean remote sites and increase in the cities. Atmos Environ 79, 705–715.
3. Paoletti E (2006) Impacts of ozone on Mediterranean forests: a Review. Environ Pollut 144, 463–474. PMID: 16551488
4. Contran N, Paoletti E (2007) Visible foliar injury and physiological responses to ozone in Italian provenances of Fraxinus excelsior and Fornus. The Scientific World Journal 7, 90–97.
5. Screpanti A, De Marco A (2009) Corrosion on cultural heritage buildings in Italy: A role for ozone? Environ Pollut 157, 1513–1520. doi: 10.1016/j.envpol.2008.09.046 PMID: 19026474

6. Khiem M, Ooka R, Huang H, Hayami H, Yoshikado H, Kawamoto Y (2010) Analysis of the relationship between changes in meteorological conditions and the variation in summer ozone levels over the Central Kanto area. Adv Meteorol, Article ID 349248, 13 pages.
7. Ran L, Zhao C, Geng FH, Tie X, Tang X, Li P, et al. (2009) Ozone photochemical production in urban Shanghai, China: analysis based on ground level observations. J Geophys Res 114, 15301–15317.
8. He JW, Wang YX, Hao JM, Shen LL, Wang L (2012) Variations of surface O_3 in August at a rural site near Shanghai: influences from the West Pacific subtropical high and anthropogenic emissions. Environ Sc Pollut R 19(9), 4016–4029.
9. Tang WY, Zhao CS, Geng FH, Peng L, Zhou GQ, Gao W, et al. (2008) Study of ozone "weekend effect" in Shanghai. Science in China Series D: Earth Sciences 51(9), 1354–1360.
10. Geng FH, Zhao CS, Tang X, Lu GL, Tie X (2007) Analysis of ozone and VOCs measured in Shanghai: A case study. Atmos Environ, 41(5), 989–1001.
11. Tie X, Geng F, Guenther A, Cao J, Greenberg J, Zhang RJ, et al. (2013) Megacity impacts on regional ozone formation: observations and WRF-Chem modeling for the MIRAGE-Shanghai field campaign, Atmos. Chem. Phys., 13(11), 5655–5669.
12. Wang HX, Zhou LJ, Tang XY (2006) Ozone concentrations in rural regions of the Yangtze Delta in China. J Atmos Chem 54, 255–265.
13. Platt U, Perner D, Patz HW (1979) Simultaneous measurement of atmospheric CH_2O, O_3 and NO_2 by differential optical absorption. J Geophys Res 84, 6329–6335.
14. Platt U, Perner D (1980) Direct measurements of atmospheric CH_2O, HNO_2, O_3, NO_2, and SO_2 by differential optical absorption in the near UV. J Geophys Res 85(C12), 7453–7458.
15. Platt U, Stutz J (2008) Differential Optical Absorption Spectroscopy. Principles and Applications. Springer-Verlag, Berlin Heidelberg, pp.135–158.
16. Virkkula A (1997) Performance of a differential optical absorption spectrometer for surface O_3 measurements in the Finish arctic. Atmos Environ 31, 545–555.
17. Alicke B, Platt U, Stutz J (2002) Impact of nitrous acid photolysis on the total hydroxyl radical budget during the limitation of oxidant production/Pianura Padana Produzione di Ozono study in Milan. J Geophys Res 107(D22), 8196.
18. Stutz J, Alicke B, Ackermann R, Geyer A, Wang S, White AB, et al. (2004a) Relative humidity dependence of HONO chemistry in urban areas. J Geophys Res 109, D03307.
19. Stutz J, Alicke B, Ackermann R, Geyer A, White A, Williams E (2004b) Vertical profiles of NO_3, N_2O_5, O_3, and NO_X in the nocturnal boundary layer: 1. Observations during the Texas Air Quality Study 2000. J Geophys Res 109, D12306.
20. Triantafyllou AG, Zoras S, Evagelopoulos V, Garas S, Diamantopoulos C (2008) DOAS measurements above an urban street canyon in a medium sized city. Global NEST J 10(2), 161–168.
21. Saiz-Lopez A, Adame JA, Notario A, Poblete J, Bolivar JP, Albaladejo J (2009) Year-Round Observations of NO, NO_2, O_3, SO_2 and Toluene Measured with a DOAS System in the industrial area of Puertollano, Spain. Water Air Soil Poll 200, 277–288.
22. Premuda M, Petritoli A, Masieria S, Palazzi E, Kostadinov I, Bortoli D, et al. (2013) A study of O_3 and NO_2 vertical structure in a coastal wooded zone near a metropolitan area, by means of DOAS measurements. Atmos Environ 71, 104–114.
23. Psiloglou RE, Larissi IK, Petrakis M, Paliatsos AG, Antoniou A, Loisos GV (2013) Case studies on summertime measurements of O_3, NO_2 and SO_2 with a DOAS system in an urban semi-industrial region in Athens, Greece. Environ Monit Assess 185, 7763–7774. doi: 10.1007/s10661-013-3134-2 PMID: 23430070
24. Hao N, Zhou B, Chen D, Sun Y, Gao S, Chen LM (2006) Measurements of NO_2, SO_2, O_3, benzene and toluene using differential optical absorption spectroscopy (DOAS) in Shanghai, China. Annali di Chimica 96, 365–375. PMID: 16948427
25. Hao N, Zhou B, Chen D, Chen LM (2006) Observations of nitrous acid and its relative humidity dependence in Shanghai. J Environ Sci 18(5), 910–915.
26. Li X, Wang SS, Zhou R, Zhou B (2014) Urban atmospheric formaldehyde concentrations measured by a differential optical absorption spectroscopy method. Environ Sci Process Impacts, 16(2), 291–297. doi: 10.1039/c3em00545c PMID: 24362786
27. Wang SS, Shi CZ, Zhou B, Zhao H, Wang ZR, Yang SN (2013) Observation of NO_3 radicals over Shanghai, China. Atmos Environ 70, 401–409.
28. Voigt S, Orphal J, Bogumil K, Burrows JP (2001) The temperature dependence (203–293 K) of the absorption cross sections of O_3 in the 230–850 nm region measured by Fourier-transform spectroscopy. J Photoch Photobio A 143, 1–9.

29. Voigt S, Orphal J, Burrows JP (2002) The temperature and pressure dependence of the absorption cross-sections of NO_2 in the 250–800 nm region measured by Fourier-transform spectroscopy. J Photoch Photobio A 149, 1–7.
30. Stutz J, Kim ES, Platt U, Bruno P, Perrino C, Febo A (2000) UV-visible absorption cross sections of nitrous acid. J Geophys Res 105(11), 14585–14592.
31. Meller R, Moortgat GK (2000) Temperature dependence of the absorption cross sections of formaldehyde between 223 and 323 K in the wavelength range 225–375 nm. J Geophys Res D105, 7089–7101.
32. Cheung VTF, Wang T (2001) Observational study of ozone pollution at a rural site in the Yangtze Delta of China. Atmos Environ 35(29), 4947–4958.
33. Xu X, Lin W, Wang T, Yan P, Tang J, Meng Z, et al. (2008) Long-term trend of surface ozone at a regional background station in eastern China 1991–2006: enhanced variability. Atmos Chem Phys 8 (10), 2595–2607.
34. Xu WY, Zhao CS, Ran L, Deng ZZ, Liu PF, Ma N (2011) Characteristics of pollutants and their correlation to meteorological conditions at a suburban site in the North China Plain. Atmos Chem Phys 11(9), 4353–4369.
35. Steiner AL, Davis AJ, Sillman S, Owen RC, Michalak AM, Fiore AM (2010) Observed suppression of ozone formation at extremely high temperature due to chemical and biophysical feedbacks. P Natl Acad Sci USA 107(46), 19685–19690.
36. Vautard R, Beekmann M, Desplat J, Hodzic A, Morel S (2007) Air quality in Europe during the summer of 2003 as a prototype of air quality in a warmer climate. C R Geosci 339(11–12), 747–763.
37. Safieddine S, Clerbaux C, George M, Hadji-Lazaro J, Hurtmans D, Coheur P-F, et al. (2013) Tropospheric ozone and nitrogen dioxide measurements in urban and rural regions as seen by IASI and GOME-2. J Geophys Res 118, 10555–10566.
38. Elminir HK (2005) Dependence of urban air pollutants on meteorology. Sci Total Environ 350(1–3), 225–237. PMID: 16227082
39. Zhang R, Lei W, Tie X, Hess P (2004) Industrial emissions cause extreme urban ozone diurnal variability. P Natl Acad Sci USA 101 (17), 6346–6350.
40. Jenkin ME, Clemitshaw KC (2000) Ozone and other secondary photochemical pollutants: chemical processes governing their formation in the planetary boundary layer. Atmos Environ 34(16), 2499–2527.
41. Nie W, Ding AJ, Xie YN, Xu Z, Mao H, Kerminen VM, et al. (2015) Influence of biomass burning plumes on HONO chemistry in eastern China. Atmos Chem Phys, 15(3), 1147–1159.
42. Li G, Lei W, Zavala M, Volkamer R, Dusanter S, Stevens PS, et al. (2010) Impacts of HONO sources on the photochemistry in Mexico City during the MCMA-2006/MILAGO Campaign. Atmos Chem Phys 10(14), 6551–6567.
43. Czader BH, Rappenglück B, Percell P, Byun DW, Ngan F, Kim S (2012) Modeling nitrous acid and its impact on ozone and hydroxyl radical during the Texas Air Quality Study 2006. Atmos Chem Phys 12 (15), 6939–6951.
44. Wang SS, Zhou R, Zhao H, Wang ZR, Chen LM, Zhou B, et al. (2013) Long-term observation of atmospheric nitrous acid (HONO) and its implication to local NO2 levels in Shanghai, China. Atmos Environ 77, 718–724.
45. Xue LK, Wang T, Gao J, Ding AJ, Zhou XH, Blake DR, et al. (2014) Ground-level ozone in four Chinese cities: precursors, regional transport and heterogeneous processes. Atmos Chem Phys, 14(23), 13175–13188.
46. Geng FH, Tie XX, Xu JM, Zhou GQ, Peng L, Gao W, et al. (2008) Characterizations of ozone, NOx, and VOCs measured in Shanghai, China. Atmos Environ 42(29), 6873–6883.
47. Su H, Cheng YF, Shao M, Gao DF, Yu ZY, Zeng LM, et al. (2008) Nitrous acid (HONO) and its daytime sources at a rural site during the 2004 PRIDE-PRD experiment in China. Journal of Geophysical Research, 113(D14), D14312.